

# Two-scale structure of the electron dissipation region during collisionless magnetic reconnection

M. A. Shay\*

*Department of Physics & Astronomy, 217 Sharp Lab, University of Delaware, Newark, DE 19716*

J. F. Drake, M. Swisdak

*University of Maryland, College Park, MD, 20742*

(Dated: November 1, 2018)

Particle in cell (PIC) simulations of collisionless magnetic reconnection are presented that demonstrate that the electron dissipation region develops a distinct two-scale structure along the outflow direction. The length of the electron current layer is found to decrease with decreasing electron mass, approaching the ion inertial length for a proton-electron plasma. A surprise, however, is that the electrons form a high-velocity outflow jet that remains decoupled from the magnetic field and extends large distances downstream from the x-line. The rate of reconnection remains fast in very large systems, independent of boundary conditions and the mass of electrons.

PACS numbers: Valid PACS appear here

Magnetic reconnection drives the release of magnetic energy in explosive events such as disruptions in laboratory experiments, magnetic substorms in the Earth's magnetosphere and flares in the solar corona. Reconnection in these events is typically collisionless because reconnection electric fields exceed the Dreicer runaway field. Since magnetic field lines reconnect in a boundary layer, the “dissipation region”, whose structure may limit the rate of release of energy, understanding the structure of this boundary layer and its impact on reconnection is critical to understanding the observations. Because of their ability to carry large currents the dynamics of electrons continues to be a topic of interest. Early simulations of reconnection suggested that the rate of reconnection was not sensitive to electron dynamics [1, 2] and this insensitivity was attributed to the coupling to whistler dynamics at the small spatial scales of the dissipation region [3, 4]. The results of more recent kinetic PIC simulations have called into question these results by suggesting that the electron current layer stretches along the outflow direction and the rate of reconnection drops [5, 6]. The fast rates of reconnection obtained from earlier simulations [1, 3, 7] were attributed to the influence of periodicity [5].

We present particle-in-cell (PIC) simulations with various electron masses and computational domain sizes and an analytic model that demonstrate that collisionless reconnection remains fast even in very large collisionless systems. The reconnection rate stabilizes before the periodicity of the boundary conditions can impact the dynamics. The electron current layer develops a distinct two-scale structure along the outflow direction that had not been identified in earlier simulations. The out-of-plane electron current driven by the reconnection elec-

tric field has a length that decreases with the electron mass, scaling as  $(m_e/m_i)^{3/8}$ , which extrapolates to about an ion inertial length  $d_i = c/\omega_{pi}$  for the electron-proton mass ratio. The surprise is that a jet of outflowing electrons with velocity close to the electron Alfvén speed  $c_{Ae}$  extends up to several 10's of  $d_i$  from the x-line. Remarkably, the electrons are able to jet across the magnetic field over such enormous distances because momentum transport transverse to the jet effectively “blocks” the flow of the out-of-plane current in this region. The momentum transport causing this “current blocking” effect has the same source (the off diagonal pressure tensor [1]), but is much stronger than that which balances the reconnection electric field at the x-line.

Our simulations are performed with the particle-in-cell code p3d [8, 9]. The results are presented in normalized units: the magnetic field to the asymptotic value of the reversed field, the density to the value at the center of the current sheet minus the uniform background density, velocities to the Alfvén speed  $v_A$ , lengths to the ion inertial length  $d_i$ , times to the inverse ion cyclotron frequency  $\Omega_{ci}^{-1}$ , and temperatures to  $m_i v_A^2$ . We consider a system periodic in the  $x - y$  plane where flow into and away from the x-line are parallel to  $\hat{y}$  and  $\hat{x}$ , respectively. The reconnection electric field is parallel to  $\hat{z}$ . The initial equilibrium consists of two Harris current sheets superimposed on a ambient population of uniform density. The reconnection magnetic field is given by  $B_x = \tanh[(y - L_y/4)/w_0] - \tanh[(y - 3L_y/4)/w_0] - 1$ , where  $w_0$  and  $L_y$  are the half-width of the initial current sheets and the box size in the  $\hat{y}$  direction. The electron and ion temperatures,  $T_e = 1/12$  and  $T_i = 5/12$ , are initially uniform. The initial density profile is the usual Harris form plus a uniform background of 0.2. The simulations presented here are two-dimensional, *i.e.*,  $\partial/\partial z = 0$ . Reconnection is initiated with a small initial magnetic perturbation that produces a single magnetic island on each current layer.

We have explored the dependence of the rate of recon-

\*Electronic address: shay@udel.edu;  
URL: <http://www.physics.udel.edu/~shay>

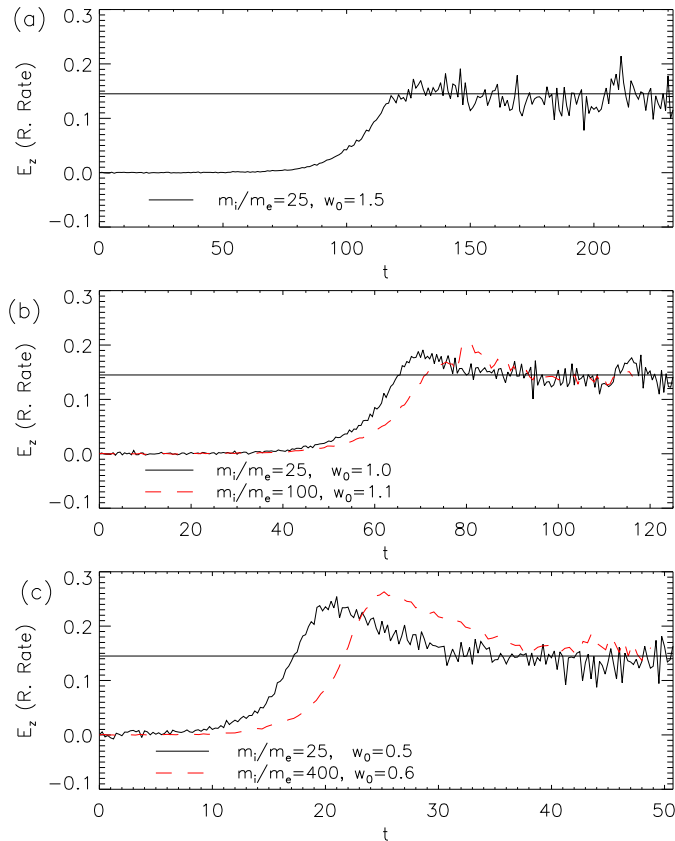


FIG. 1: (color online). Reconnection electric field versus time: (a)  $204.8 \times 102.4$ , (b)  $102.4 \times 51.2$ , (c)  $51.2 \times 25.6$ .  $w_0$  is the initial current sheet width.

nection on the system size in a series of simulations with three different system sizes and three different mass ratios. For  $m_i/m_e = 25$ , the grid scale  $\Delta = 0.05$  and the speed of light  $c = 15$ . For  $m_i/m_e = 100$ ,  $\Delta = 0.025$  and  $c = 20$ . For  $m_i/m_e = 400$ ,  $\Delta = 0.0125$  and  $c = 40$ . The reconnection rate versus time is plotted for our simulations in Fig. 1. The reconnection rate is determined by taking the time derivative of the total magnetic flux between the x-line and the center of the magnetic island. The rate increases with time, undergoes a modest overshoot that is more pronounced in the smaller domains, and approaches a quasi-steady rate of around 0.14, independent of the domain size. Earlier suggestions [5] that reconnection rates would plunge until elongated current layers spawned secondary magnetic islands are not borne out in these simulations. The rates of reconnection approach constant values even in the absence of secondary islands, which for anti-parallel reconnection typically only occur transiently due to initial conditions[10]. Even these transient islands can be largely eliminated by a suitable choice of the initial current layer width  $w_0$  (a larger value of  $w_0$  is required for the larger domains).

A critical issue is whether the periodicity in the  $x$  direction can influence the rate of reconnection [5]. In each of the simulations we have identified the time at which the

ion outflows from the x-line meet at the center of the magnetic island. This occurs at  $t \approx 155$  for the largest simulation shown in Fig. 1a. The plasma at the x-line can not be affected by the downstream conditions until  $t \approx 255$ , when a pressure perturbation can propagate back upstream to the x-line at the magnetosonic speed. This is well after the end of the simulation. The electrons are ejected from the x-line at a velocity of around  $c_{Ae} \gg c_A$  and therefore might be able to follow field lines back to the x-line. During the traversal time  $\delta t = L_x/c_{Ae}$ , the amount of reconnected flux is  $v_{in}B_0L/c_{Ae}$ , where  $v_{in}$  is the inflow velocity into the x-line. Using the conservation of the canonical momentum in the  $z$ -direction, the condition that an electron with a velocity  $c_{Ae}$  can not cross this flux to access the x-line reduces to  $L > d_i(c_A/v_{in}) \sim 7d_i$ , which is easily satisfied for the simulations in Fig. 1. The fact that the reconnection rates for all of the simulation domains in Fig. 1 are essentially identical further supports this conclusion.

Also shown in Fig. 1 in the dashed lines are the rates of reconnection for  $m_i/m_e = 100$  in (b) and  $m_i/m_e = 400$  in (c). Consistent with simulations in smaller domains [1, 2], the rate of reconnection is insensitive to the electron mass.

We now proceed to explore the structure of the electron current layer. Shown in Fig. 2 is a blow-up around the x-line of the out-of-plane electron velocity for  $m_i/m_e = 25$  and two simulation domains,  $204.8 \times 102.4$  in (a) and  $51.2 \times 25.6$  in (b), and for  $m_i/m_e = 400$  in a simulation domain of  $51.2 \times 25.6$  in (c). All of the data is taken in the phase where the reconnection rate and the lengths of the region of intense out-of-plane current are stationary. Reconnection forms intense current layers that have a well-defined length (half widths of around  $7d_i$  and independent of the size of computational domain for  $m_i/m_e = 25$ ) and then open up forming the open outflow jet that characterizes Hall reconnection [3, 7]. The current layer in the case of  $m_i/m_e = 400$  in Fig. 2c is distinctly shorter than the smaller mass ratio current layers in Fig. 2a,b, suggesting that the length of the electron current layer depends on the electron mass and would be shorter for realistic proton-electron mass ratios.

Shown in Fig. 3a is a blow-up around the x-line of the electron outflow velocity  $v_{ex}$  for the  $m_i/m_e = 25$ ,  $204.8 \times 102.4$  run corresponding to Fig. 2a. In contrast with the out-of-plane current the electrons form an outflow jet that extends a very large distance downstream from the x-line. This outflow jet continued to grow in length until the end of the simulation. This simulation, along with others at differing mass ratios, reveals that the peak outflow velocity is very close to the electron Alfvén speed [8, 11]. One might expect that because of the collimation of the outflow jet and its length, the reconnection rate would drop. However, this is not the case. While there is an intense jet in the core of the reconnection exhaust, the exhaust as a whole quickly begins to open up downstream of the current layer ( $J_z$ ). The jet itself therefore does not act as a nozzle to limit the rate of

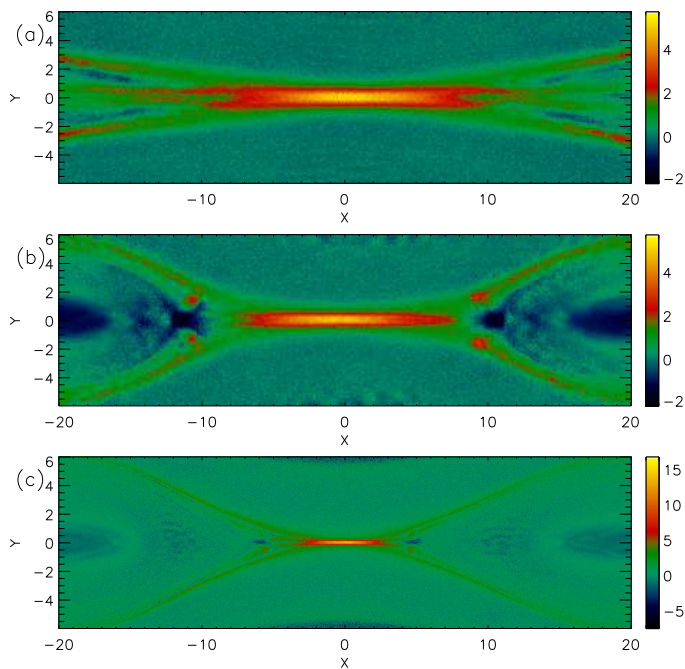


FIG. 2: (color online). Blowups around the x-line of the out-of-plane electron velocity for: (a)  $m_i/m_e = 25$ , simulation size  $204.8 \times 102.4$ , (b)  $m_i/m_e = 25$ ,  $51.2 \times 25.6$ , and (c)  $m_i/m_e = 400$ ,  $51.2 \times 25.6$ .

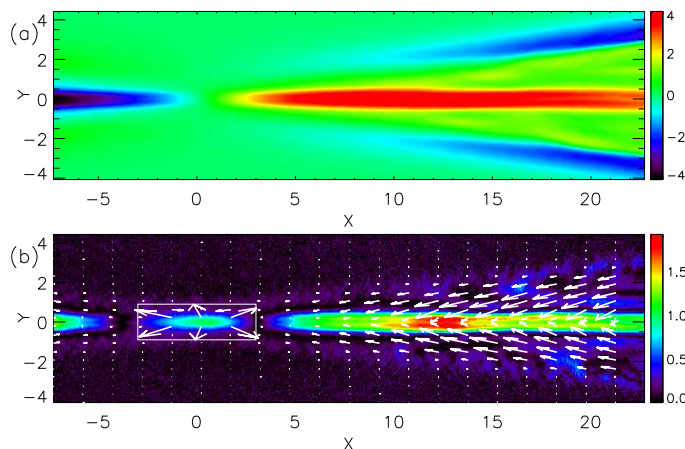


FIG. 3: (color online). Blowups around the x-line for system size  $204.8 \times 102.4$  with  $m_i/m_e = 25$ . (a) The electron outflow velocity  $v_{ex}$ . (b) Momentum flux vectors,  $\mathbf{\Gamma} = p_{exz}\hat{\mathbf{x}} + p_{eyz}\hat{\mathbf{y}}$  (vectors in box surrounding x-line are multiplied by 20), with a background color plot of  $|(E_z + (\mathbf{v}_e \times \mathbf{B}/c)_z)/E_z|$ .

reconnection: the rate of reconnection remains constant even as the length of the outflow jet varies in time.

To understand how the electrons can form such an extended outflow jet while the out-of-plane current layer remains localized, we examine the out-of-plane component of the fluid electron momentum equation along the

symmetry line of the outflow direction. In steady state

$$E_z = -\frac{m_e v_{ex}}{e} \frac{\partial v_{ez}}{\partial x} - \frac{1}{c} v_{ex} B_y - \frac{1}{ne} \nabla \cdot \mathbf{\Gamma}, \quad (1)$$

where  $\mathbf{v}_e$  is the electron bulk velocity,  $\mathbf{\Gamma} = p_{exz}\hat{\mathbf{x}} + p_{eyz}\hat{\mathbf{y}}$  is the flux of z-directed electron momentum in the reconnection plane (not including convection of momentum) with  $\mathbf{p}_e$  the electron pressure tensor. In Fig. 4a we plot all of the terms in this equation along a cut through the x-line along the outflow direction from a simulation with  $m_i/m_e = 100$  and  $L_x \times L_y = 102.4 \times 51.2$ . The data has been averaged between  $t = 116.2$  and  $t = 117.0$ . The electric field (black) is balanced by the sum (red) of the electron inertia (dashed blue), the Lorentz force (solid blue) and the divergence of the momentum flux (green). The major contributions to momentum balance come from the Lorentz force and the divergence of the momentum flux. At the x-line the electric field drive is balanced by the momentum transport [1, 12]. The surprise is that the Lorentz force, rather than simply increasing downstream from the x-line to balance the reconnection electric field, instead strongly overshoots the reconnection electric field far downstream of x-line. This tendency was seen in earlier simulations [12] but there was no clear separation of scales because of the small size of these earlier simulations. Downstream from the x-line the electrons are streaming much faster than the magnetic field lines. Thus, in a reference frame of the moving electrons the z-directed electric field has reversed direction compared with the x-line. This electric field tries to drive a current opposite to that at the x-line. Evidence for this reversed current appears downstream of the x-line in Fig. 2c. In spite of the strength of the effective electric field, the reversed current carried by the electrons is small. As at the x-line, the momentum transfer to electrons in this extended outflow region is balanced by momentum transport. The momentum flux around the x-line is shown as a 2-D vector plot in Fig. 3 for the same run as in (a). The momentum flux has been multiplied by 20 in the box surrounding the x-line. The data for this figure has been averaged between  $t = 172.5$  and  $174.5$ . The background color plot is of  $|(E_z + (\mathbf{v}_e \times \mathbf{B}/c)_z)/E_z|$ , which is  $\gtrsim 1$  where the electrons are not frozen-in. Evident is the outward flow of momentum around the x-line and the much stronger outward flow of negative momentum in an extended downstream region. The momentum transport is so large that the out-of-plane current downstream is effectively “blocked”. The force associated with this “blocking effect” drives the flow of the large-scale jet of electrons downstream of the x-line.

We define the length  $\Delta_x$  of the inner dissipation region as the distance from the x-line to the point where the Lorentz force  $v_{ex}B_y/c$  crosses the reconnection electric field  $E_z$ . At this location the effective out-of-plane electric field seen by the electrons reverses sign, causing the electron current  $j_{ez}$  to be driven in reverse, which allows the separatrix to open up. Thus, the inner dissipation region defines the spatial extent of the magnetic

nozzle that develops during reconnection. Since the simulations presented in this paper use artificial values of  $m_e$ , it is essential to understand the  $m_e$  scaling of  $\Delta_x$  so that this important length can be calculated for a proton-electron plasma. The momentum equation of electrons in the outflow direction yields a steady state equation for  $v_{ex}$ ,

$$\frac{d}{dx} \left( \frac{1}{2} m_e v_{ex}^2 \right) = \frac{e}{c} v_{ez} B_y, \quad (2)$$

where  $v_{ez} \sim c_{Ae}$ . Thus, the profile of  $B_y$  along the outflow direction and its dependence on  $m_e$  must be determined. This profile is shown for  $m_i/m_e = 25$  (system size  $102.4 \times 51.2$ ), 100 ( $102.4 \times 51.2$ ) and 400 ( $51.2 \times 25.6$ ) in Fig. 4b. Surprisingly, the profile of  $B_y$  is apparently independent of  $m_e$ . Our original expectation was because of the continuity of the flow of magnetic flux into and out of the x-line that  $B_y \sim B_0 v_{in}/c_{Ae} \propto m_e^{1/2}$ , where the outflow velocity eventually rises to  $c_{Ae}$ . However, since the electrons are not frozen into the magnetic field until far downstream, the expected scaling fails. To calculate  $v_{ex}$  we approximate  $B_y$  by a linear ramp and integrate Eq. (2). Setting the Lorentz force equation to the reconnection electric field, we then obtain an equation for  $\Delta_x$ ,

$$\Delta_x = \left( \frac{m_e}{m_i} \right)^{3/8} \left( \frac{cE_z}{B_0 c_A} \right)^{1/2} \left( \frac{B_0}{d_i B_y'} \right) d_i. \quad (3)$$

For the three simulations shown in Fig. 4b the simulations yield  $2.9d_i$ ,  $1.8d_i$  and  $1.0d_i$  for  $m_i/m_e = 25$ , 100 and 400, respectively, which is in reasonable accord with the scaling. Extrapolating to a mass-ratio of 1836, we predict  $\Delta_x \sim 0.6d_i$ . In contrast the outer dissipation region can extend to 10's of  $d_i$ .

We have shown that the electron current layer that forms during reconnection stabilizes at a finite length, independent of the periodicity of the simulation domain, and aside from transients from initial conditions remains largely stable to secondary island formation. Reconnection remains fast with normalized reconnection rates of around 0.14. The length of the electron current layer  $\Delta_x$  scales as  $m_e^{3/8}$ . Since the width  $\delta$  of the current layer scales with the electron skin depth  $c/\omega_{pe}$ , the aspect-ratio  $\delta/\Delta_x \propto (m_e/m_i)^{1/8}$ . Extrapolating from our  $m_i/m_e = 400$  simulations to  $m_i/m_e = 1836$  should not

significantly change the aspect-ratio and we therefore expect the current layer to remain stable for real mass ratios.

The structure of the current layer is important to the design of NASA's magnetospheric multiscale mission (MMS), which will be the first mission with the time resolution to measure the electron current layers that develop during reconnection. The length of the out-of-plane electron current layer projects to around  $c/\omega_{pi}$  for a proton-electron plasma while the the outflow jet, which supports a strong Hall (out-of-plane) magnetic field, extends 10's of  $c/\omega_{pi}$  from the x-line.

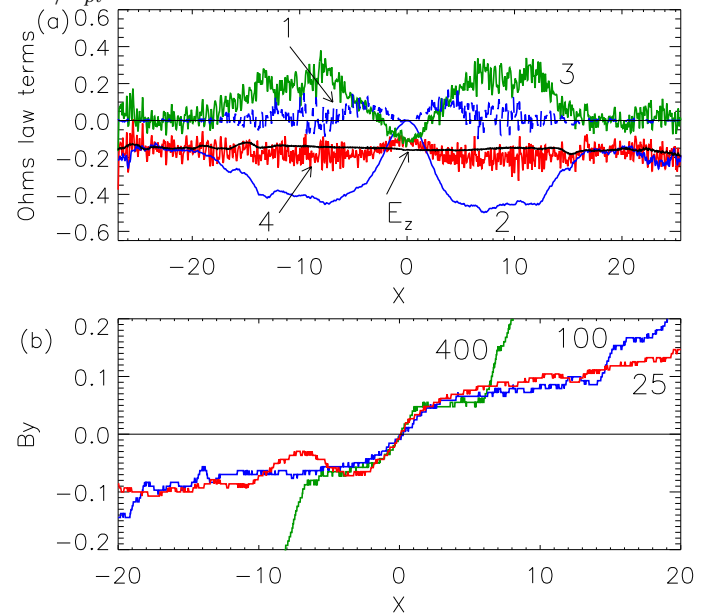


FIG. 4: (color online). Results for simulation size  $102.4 \times 51.2$  with  $m_i/m_e = 25$  and 100; and  $51.2 \times 25.6$  with  $m_i/m_e = 400$ . (a) Cuts through the x-line of the contributions to Ohm's law for  $m_i/m_e = 100$ . 1  $\rightarrow -m_e/e\mathbf{v}_e \cdot \nabla v_{ez}$ , 2  $\rightarrow -\hat{\mathbf{z}} \cdot \mathbf{v}_e \times \mathbf{B}/e$ , 3  $\rightarrow -\hat{\mathbf{z}} \cdot (\nabla \cdot \mathbf{P}_e)/(n_e e)$ , 4  $\rightarrow$  sum of 1,2,3. (b) Cuts through x-line of  $B_y$  for the three different  $m_i/m_e$ .

This work was supported in part by NSF, NASA and DOE.

**Acknowledgments** This work was supported in part by NASA and the NSF. Computations were carried out at the National Energy Research Scientific Computing Center.

[1] M. Hesse *et al.*, Phys. Plasmas **6**, 1781 (1999).  
 [2] M. A. Shay and J. F. Drake, Geophys. Res. Lett. **25**, 3759 (1998).  
 [3] J. Birn *et al.*, J. Geophys. Res. **106**, 3715 (2001).  
 [4] B. N. Rogers *et al.*, Phys. Rev. Lett. **87**, 195004 (2001).  
 [5] W. Daughton *et al.*, Phys. Plasmas **13**, 072101 (2006).  
 [6] K. Fujimoto, Phys. Plasmas **13**, 072904 (2006).  
 [7] M. A. Shay *et al.*, Geophys. Res. Lett. **26**, 2163 (1999).

[8] M. A. Shay *et al.*, J. Geophys. Res. **106**, 3751 (2001).  
 [9] A. Zeiler *et al.*, J. Geophys. Res. **107**, 1230 (2002), doi:10.1029/2001JA000287.  
 [10] J. F. Drake *et al.*, Geophys. Res. Lett. **33**, L13105 (2006), doi:10.1029/2006GL025957.  
 [11] M. Hoshino *et al.*, J. Geophys. Res. **106**, 25979 (2001).  
 [12] P. L. Pritchett, J. Geophys. Res. **106**, 3783 (2001).